The Influence of Boundary Conditions on NIMROD Axisymmetric VDE Computations

Theory and Simulation of Disruptions Conference 2019

K. J. Bunkers and C. R. Sovinec

University of Wisconsin-Madison

Table of Contents

Vertical Displacement Events (VDEs) are sensitive to edge plasma modeling.

- Halo-plasma modeling strongly influences the evolution of VDEs.
- The halo temperature controls plasma resistivity, and thus affects vertical movement.
- The thermal conduction properties of this region are important for accurate modeling.

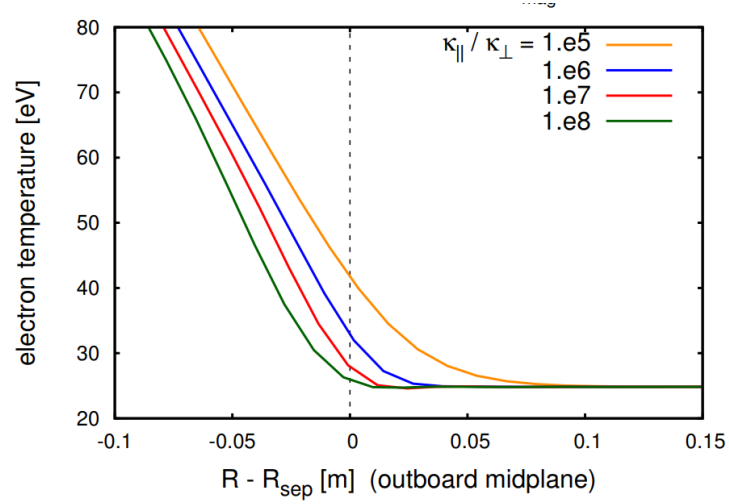

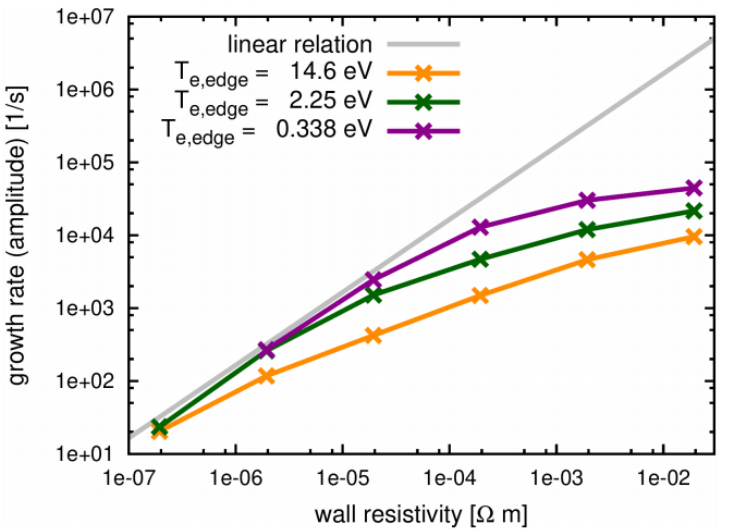

Halo temperature sensitivity to the thermal heat conduction ratio $\kappa_{\|}/\kappa_{\perp}$ and edge temperature in M3D-C^1 from I. Krebs, *IAEA Poster*, 2018.

Previous work investigated sensitivity to varying the flow-velocity boundary conditions.

- The velocity boundary condition has been considered previously.
  - Zakharov's tokamak MHD implies that $\mathbf{E}_{\text{wall}} \times \mathbf{B}$ drift is relevant.[1]
  - Strauss implemented this flow and saw minimal changes to the force with respect to $\mathbf{V} = \mathbf{0}$.[2]
- However, Strauss noted that a Neumann velocity boundary condition $\nabla(\mathbf{V} \cdot \hat{\mathbf{n}}) = \mathbf{0}$ did increase the forces seen in calculations.

[1] Zakharov, et. al., *PoP* 19(5), 2012.
[2] Strauss, *PoP* 21(3), 2014.

We have considered more detailed modeling using MPS[a] boundaries and Braginskii thermal conduction.

- The velocity boundary condition is a Chodura-Bohm condition directed along the magnetic field lines at c_s.[3]
- The electron temperature uses an insulating boundary condition.
- The thermal conduction is given by the Braginskii model in low-temperature plasma regions.

[3] Chodura, *Phys Fl*, 25(9) (1982)

[a] magnetic presheath

Table of Contents

We have used forced VDE computations to investigate the effects of various boundary conditions.

- The equilibrium pressure with poloidal flux contours for the central plasma region is shown in the upper right.
- We use two coupled domains for resistive wall calculations.
- The VDE is created by turning off a divertor coil and letting the induced currents in the resistive wall decay.
- A Spitzer resistivity model $\eta(T_e) = \eta_0 T_e^{-3/2}$ distinguishes high and low conductivity plasma.

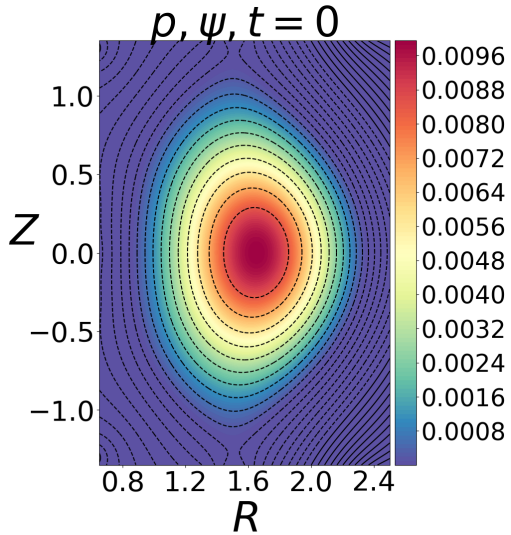

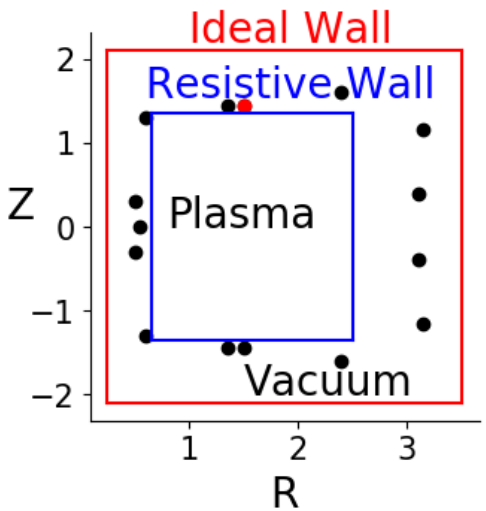

The NIMROD equations are evolved for this axisymmetric calculation.

$$\frac{\partial n}{\partial t} + \boldsymbol{\nabla}\cdot(n\mathbf{V}) = \boldsymbol{\nabla}\cdot(D_n\nabla n - D_h\nabla\nabla^2 n)$$

Continuity with diffusive numerical fluxes

$$mn\left(\frac{\partial}{\partial t} + \mathbf{V}\cdot\nabla\right)\mathbf{V} = \mathbf{J}\times\mathbf{B} - \nabla p - \boldsymbol{\nabla}\cdot\overleftrightarrow{\boldsymbol{\Pi}}$$

flow evolution

$$\frac{3}{2}n\left(\frac{\partial}{\partial t} + \mathbf{V}\cdot\nabla\right)T_s = -nT_s\boldsymbol{\nabla}\cdot\mathbf{V} - \boldsymbol{\nabla}\cdot\mathbf{q}_s$$

temperature evolution

$$\frac{\partial \mathbf{B}}{\partial t} = -\boldsymbol{\nabla}\times(\eta\mathbf{J} - \mathbf{V}\times\mathbf{B}) + \kappa_B\nabla\boldsymbol{\nabla}\cdot\mathbf{B}$$

Faraday's/Ohm's Law with numerical error control

$$\mu_0\mathbf{J} = \boldsymbol{\nabla}\times\mathbf{B}$$

low-ω Ampere's law

$$\overleftrightarrow{\boldsymbol{\Pi}} = -\rho\nu\overleftrightarrow{\mathbf{W}} - \rho\nu_{\parallel}\overleftrightarrow{\mathbf{W}}_{\parallel}, \quad \overleftrightarrow{\mathbf{W}} = \nabla\mathbf{V} + (\nabla\mathbf{V})^{\mathsf{T}} - \frac{2}{3}\mathbb{1}(\boldsymbol{\nabla}\cdot\mathbf{V})$$

The thermal diffusivity coefficients can either be fixed, Braginskii, or "k2".

- For fixed coefficients, then $\mathbf{q}_s = \kappa_{\perp,s} \nabla_\perp T_s + \kappa_{\parallel,s} \nabla_\parallel T_s$ with the κ/n being constants in time and space.
- For the Braginskii (left) and "k2" model[4] (right), the coefficients are specified through thermal diffusivities $\chi = \kappa/n$

$$\chi^B_{\parallel,s} = \frac{T_s \tau_s}{m_s} \frac{\gamma_{0,s}}{\delta_{0,s}}$$

$$\chi^B_{\perp,s} = \frac{T_s \tau_s}{m_s} \frac{\gamma_{1,s} x_s^2 + \gamma_{0,s}}{x_s^4 + \delta_{1,s} x_s^2 + \delta_{0,s}}$$

$$\tau^B_e = \frac{12\pi^{3/2}\sqrt{m_e}\, T_e^{3/2} \epsilon_0^2}{\sqrt{2} n_e e^4 \ln \Lambda}$$

$$\tau^B_i = \frac{12\pi^{3/2}\sqrt{m_i}\, T_i^{3/2} \epsilon_0^2}{n_e e^4 \ln \Lambda}$$

$$\boxed{x_s = \Omega_s \tau_s}$$

$$\chi^{k2}_{\parallel,e} = \frac{T_e \tau_e}{m_e} \hat{k}_{\parallel,e} \quad \chi^{k2}_{\parallel,i} = \frac{T_i \tau_i}{m_i} \hat{k}_{\parallel,i}$$

$$\chi^{k2}_{\perp,e} = \frac{T_e \tau_e}{m_e} f(x_e, Z_{\text{eff}})$$

$$\chi^{k2}_{\perp,i} = \frac{T_i \tau_i}{m_i} g(x_i, Z_{\text{eff}}, \frac{T_i}{T_e})$$

$$\tau^{k2}_i = \tau^B_i / \sqrt{2}$$

[4] Ji, PoP (2013)

The T-dependent thermal diffusivity is cutoff at high temperatures.

- The thermal diffusivity parameters are cutoff from above at around 10 eV.
- Some are run with a lower bound on diffusivity so that they would not decrease below $1\,\mathrm{m}^2/\mathrm{s}$ in a physically relevant case.

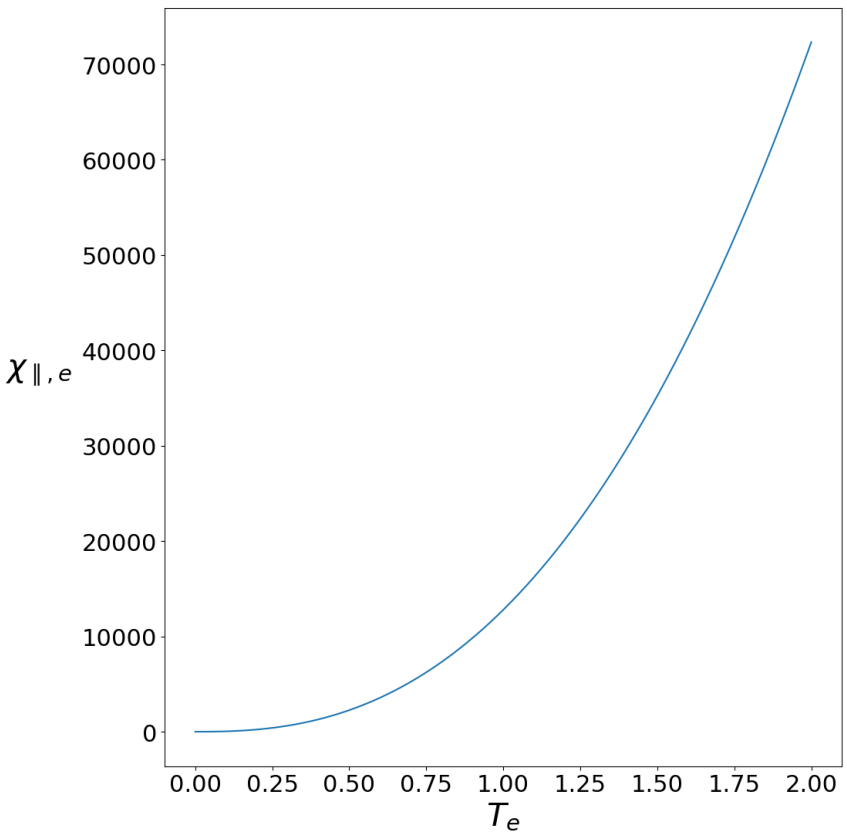

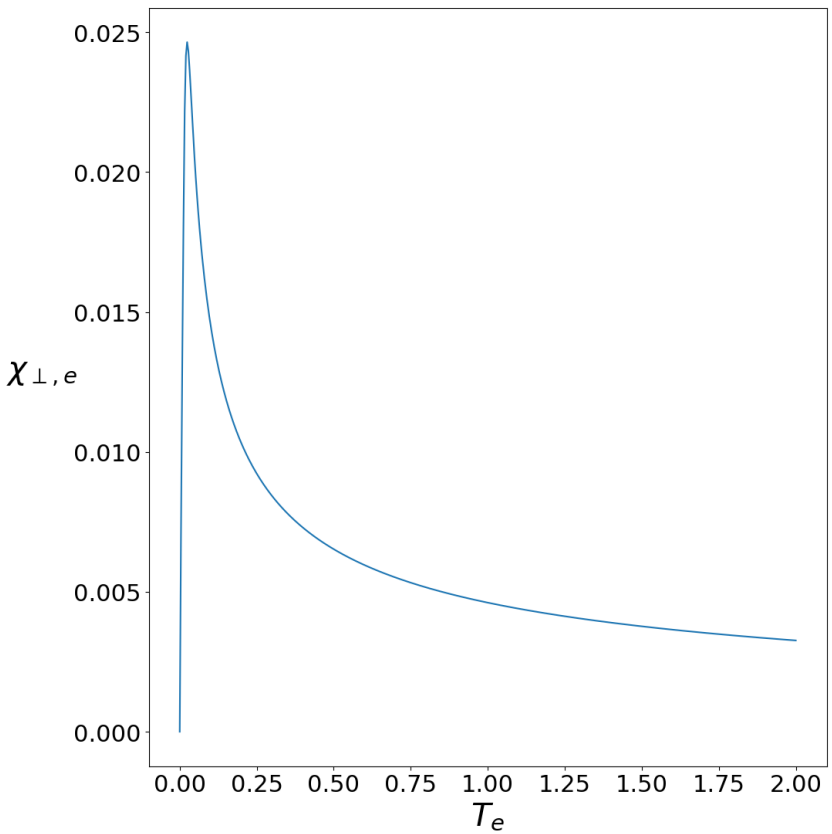

A magnetic presheath model[5] yields relations for boundary conditions.

- In the zeroth order ($\rho_s/L \to 0$) approximation, with $\mathbf{V}$ the ion velocity and MPE meaning the magnetic presheath entrance value.

$$\hat{\mathbf{s}} \cdot \mathbf{V}_{\mathrm{MPE}} = c_s \hat{\mathbf{n}} \cdot \hat{\mathbf{b}}_{\mathrm{MPE}}, \quad \hat{\mathbf{n}} \cdot \nabla T_e = 0$$

$$[6] \Rightarrow \hat{\mathbf{n}} \cdot \mathbf{J}_{\mathrm{MPE}} = enc_s \sin\alpha(1 - \exp[\Lambda - \eta])$$

- The velocity boundary condition is the well-known Chodura-Bohm criterion[3].

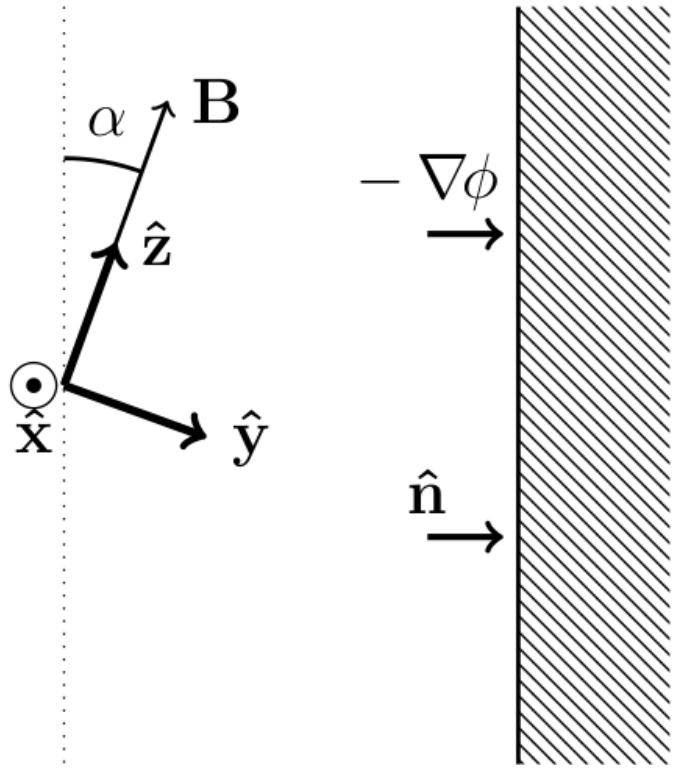

Magnetic presheath coordinate directions.

[3] Chodura, *Phys Fl*, 25(9), (1982)
[5] Loizu, et al., *PoP* 19(12), (2012)
[6] Cohen and Ryutov, *PoP* 2(6), (1995)

Table of Contents

Our most comprehensive model serves as a base case for comparison.

- The model uses the MPS boundary conditions and the Braginskii thermal conduction model.
- The plasma decays away within $8\tau_w$, with a resistive wall time of $\tau_w = a\mu_0\delta_w/\eta_w \approx 1000\tau_A$.

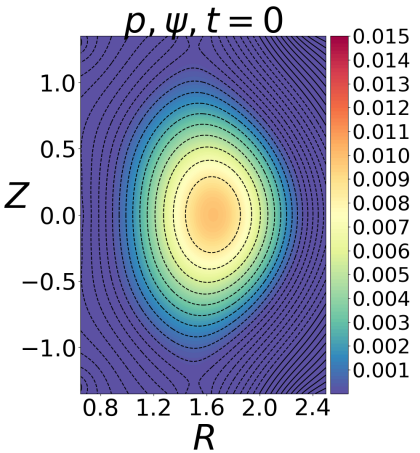

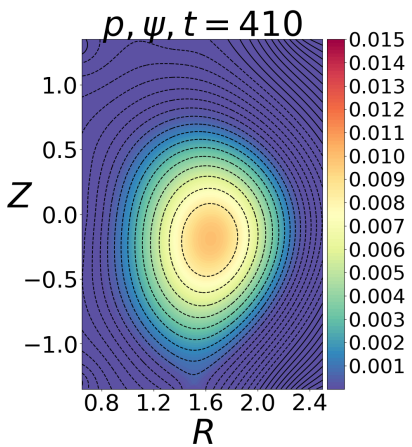

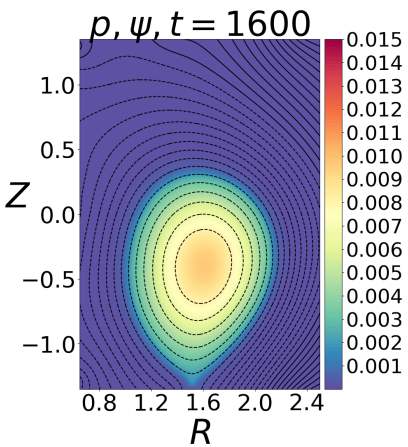

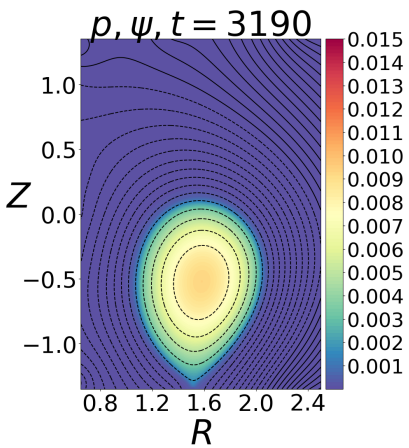

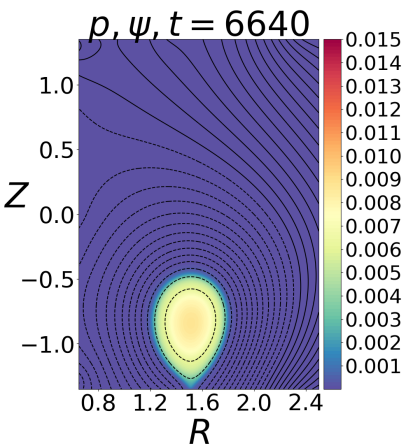

A visual aid helps chart the parameter space we have considered.

Quantity	Condition Name	Shorthand	Description
$\mathbf{V}$	$\mathbf{E}\times\mathbf{B}$	EB	$\mathbf{V}_s = \hat{\mathbf{s}}\cdot\mathbf{E}\times\mathbf{B}/B^2$
$\mathbf{V}$	Chodura-Bohm and $\mathbf{E}\times\mathbf{B}$	CB+	$\mathbf{V} = \pm c_s\mathbf{b} + \mathbf{E}\times\mathbf{B}/B^2$
T_s	insulate	I	$\mathbf{q}_s = \mathbf{0}$
T_s	Dirichlet	D	$T_s = T_{\text{edge}}$
n	Dirichlet	D	$n = n_{\text{edge}}$
χ	fixed	F	$\chi_{\perp,\parallel}$ = constant
χ	fixed	T	$\chi_{\perp,\parallel,i,e}$ = constant
χ	Braginskii	B	$\chi = \chi^B$
χ	k2	$k2$	$\chi = \chi^{k2}$

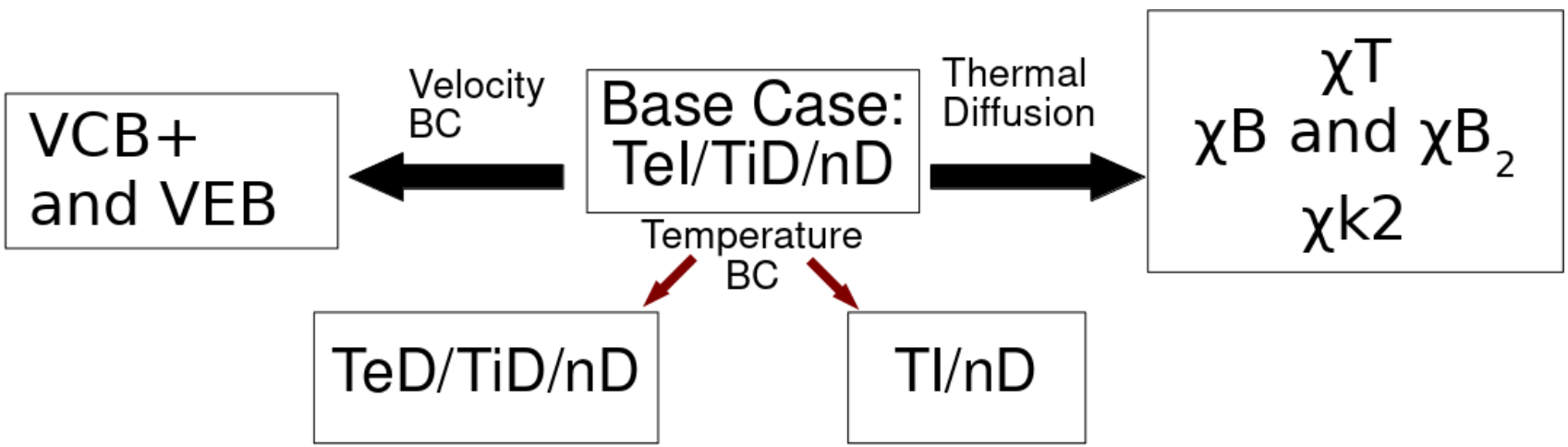

The comparison among different thermal diffusion models will be presented.

Quantity	Condition Name	Shorthand	Description
$\mathbf{V}$	$\mathbf{E}\times\mathbf{B}$	EB	$\mathbf{V}_s = \hat{\mathbf{s}}\cdot\mathbf{E}\times\mathbf{B}/B^2$
$\mathbf{V}$	Chodura-Bohm and $\mathbf{E}\times\mathbf{B}$	CB+	$\mathbf{V} = \pm c_s\mathbf{b} + \mathbf{E}\times\mathbf{B}/B^2$
T_s	insulate	I	$\mathbf{q}_s = \mathbf{0}$
T_s	Dirichlet	D	$T_s = T_{\text{edge}}$
n	Dirichlet	D	$n = n_{\text{edge}}$
χ	fixed	F	$\chi_{\perp,\parallel}$ = constant
χ	fixed	T	$\chi_{\perp,\parallel,i,e}$ = constant
χ	Braginskii	B	$\chi = \chi^B$
χ	k2	$k2$	$\chi = \chi^{k2}$

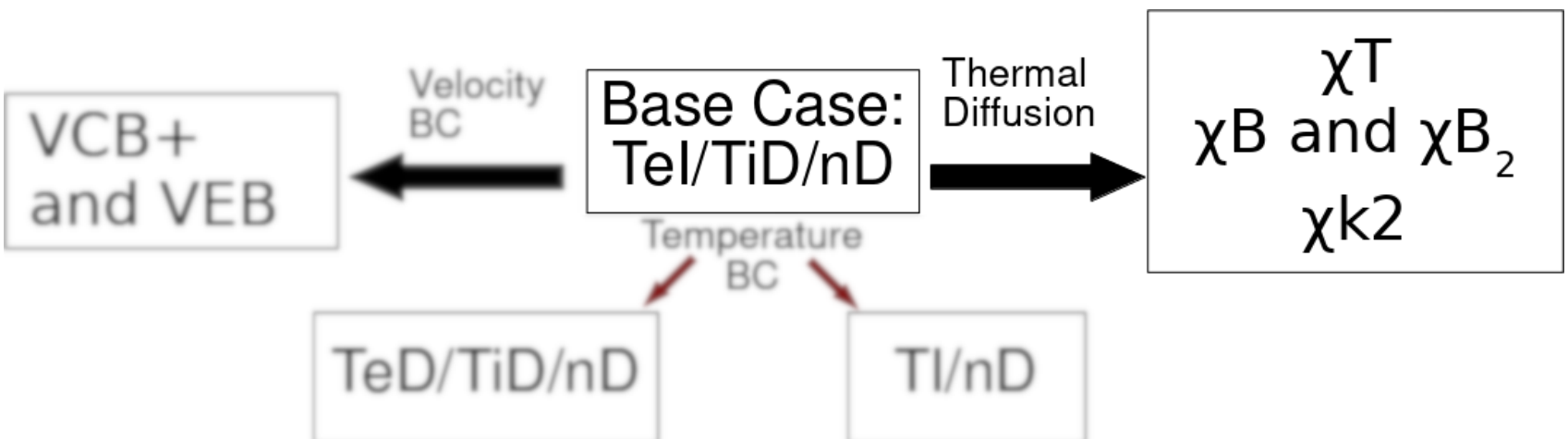

The models with large perpendicular thermal diffusion show slower VDE decay of current and internal energy.

- The current and internal energy ($\int \mathrm{d}V\ p/(\gamma-1)$) are shown for different thermal conduction models.
- The changes in $\kappa_\perp$ affect the resistivity profile, broadening the halo region, and leading to a slower decay in these forced VDEs.

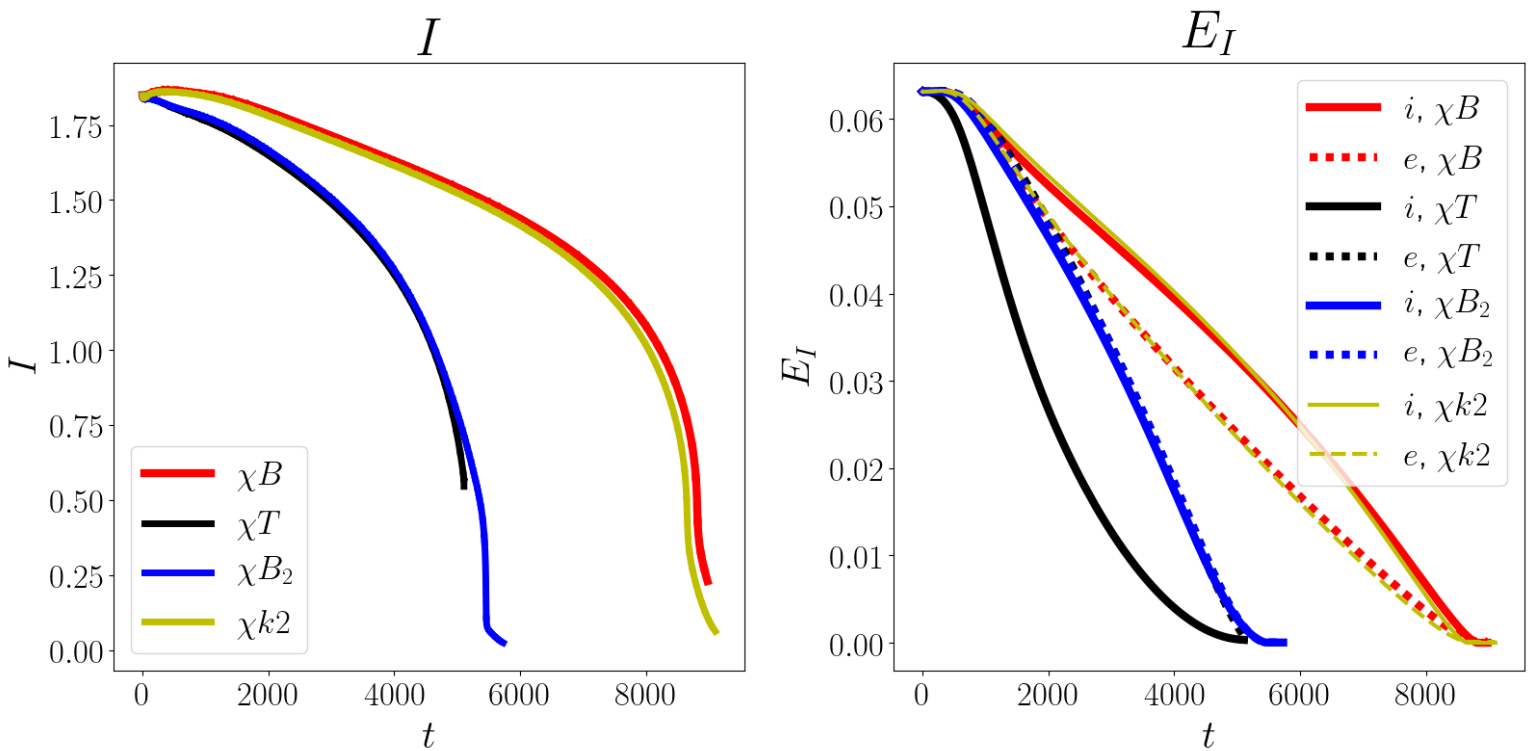

The halo regions are broadened when increasing the perpendicular thermal conduction.

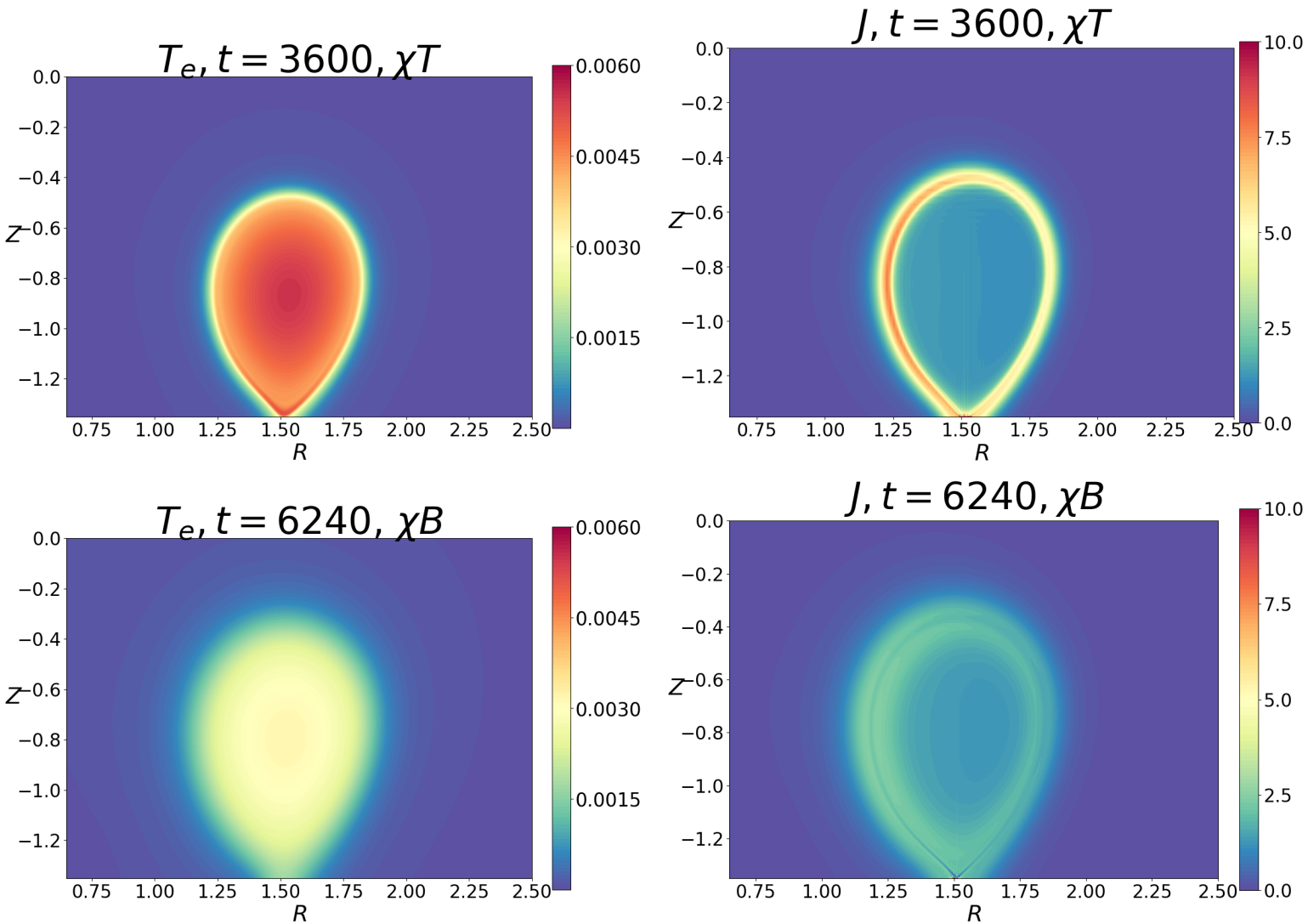

The comparison with velocity boundary conditions will be presented next.

Quantity	Condition Name	Shorthand	Description
$\mathbf{V}$	$\mathbf{E}\times\mathbf{B}$	EB	$\mathbf{V}_s = \hat{\mathbf{s}}\cdot\mathbf{E}\times\mathbf{B}/B^2$
$\mathbf{V}$	Chodura-Bohm and $\mathbf{E}\times\mathbf{B}$	CB+	$\mathbf{V} = \pm c_s\mathbf{b} + \mathbf{E}\times\mathbf{B}/B^2$
T_s	insulate	I	$\mathbf{q}_s = \mathbf{0}$
T_s	Dirichlet	D	$T_s = T_{\text{edge}}$
n	Dirichlet	D	$n = n_{\text{edge}}$
χ	fixed	F	$\chi_{\perp,\parallel}$ = constant
χ	fixed	T	$\chi_{\perp,\parallel,i,e}$ = constant
χ	Braginskii	B	$\chi = \chi^B$
χ	k2	$k2$	$\chi = \chi^{k2}$

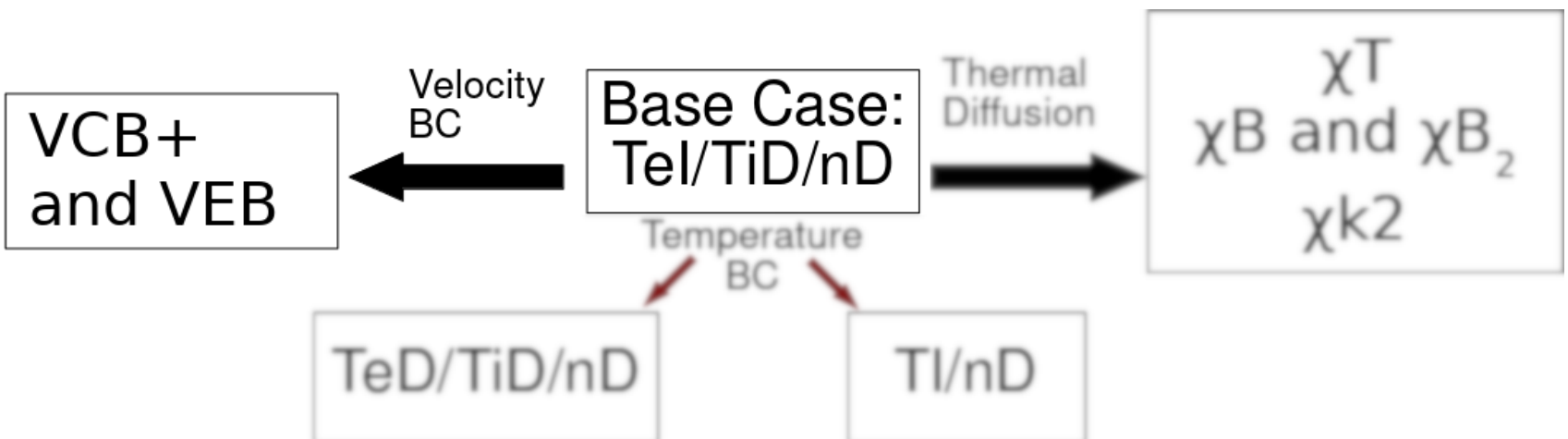

The Chodura-Bohm velocity boundary condition shortens the termination time.

- The pure **E** $\times$ **B** drift condition decays much more slowly.

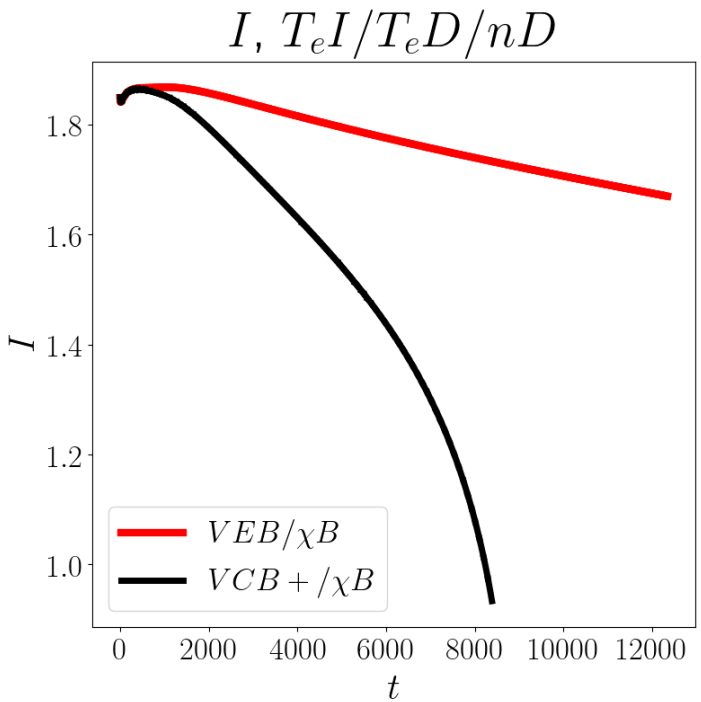

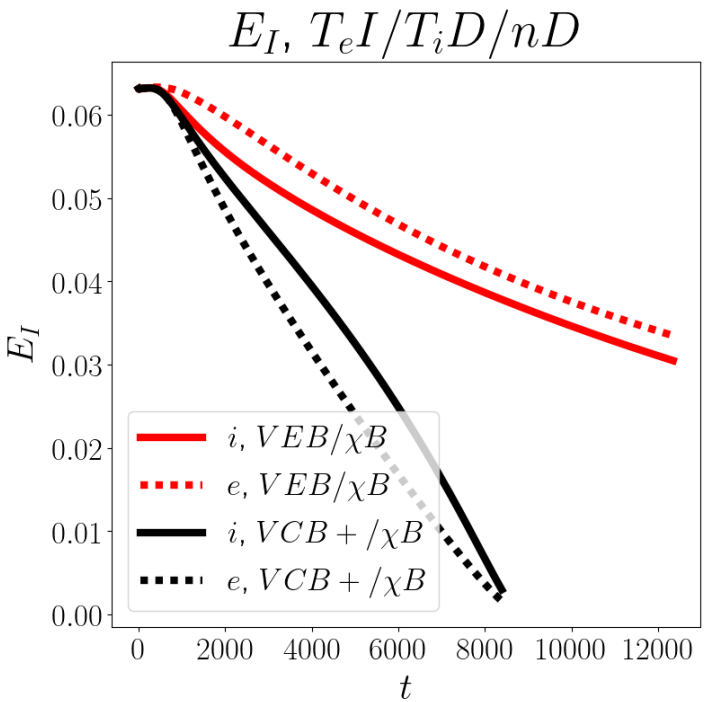

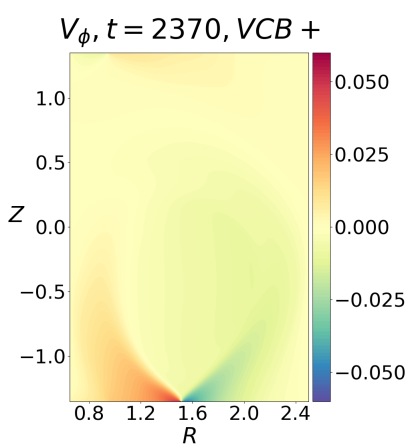

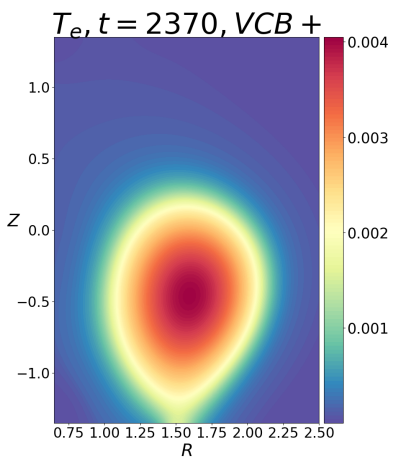

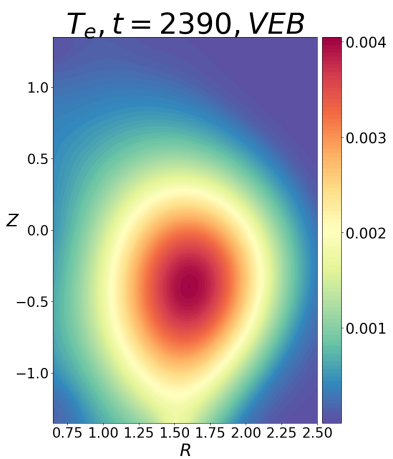

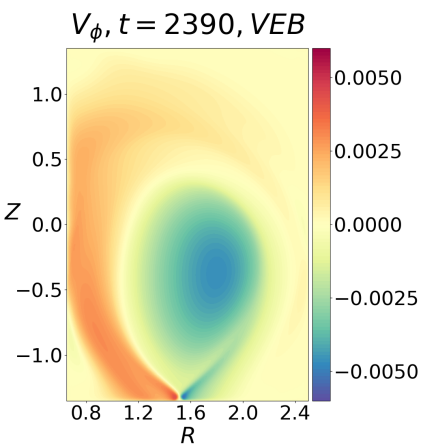

The comparison of temperature boundary conditions will now be presented.

Quantity	Condition Name	Shorthand	Description
$\mathbf{V}$	$\mathbf{E}\times\mathbf{B}$	EB	$\mathbf{V}_s = \hat{\mathbf{s}}\cdot\mathbf{E}\times\mathbf{B}/B^2$
$\mathbf{V}$	Chodura-Bohm and $\mathbf{E}\times\mathbf{B}$	CB+	$\mathbf{V} = \pm c_s\mathbf{b} + \mathbf{E}\times\mathbf{B}/B^2$
T_s	insulate	I	$\mathbf{q}_s = \mathbf{0}$
T_s	Dirichlet	D	$T_s = T_{\text{edge}}$
n	Dirichlet	D	$n = n_{\text{edge}}$
χ	fixed	F	$\chi_{\perp,\parallel}$ = constant
χ	fixed	T	$\chi_{\perp,\parallel,i,e}$ = constant
χ	Braginskii	B	$\chi = \chi^B$
χ	k2	$k2$	$\chi = \chi^{k2}$

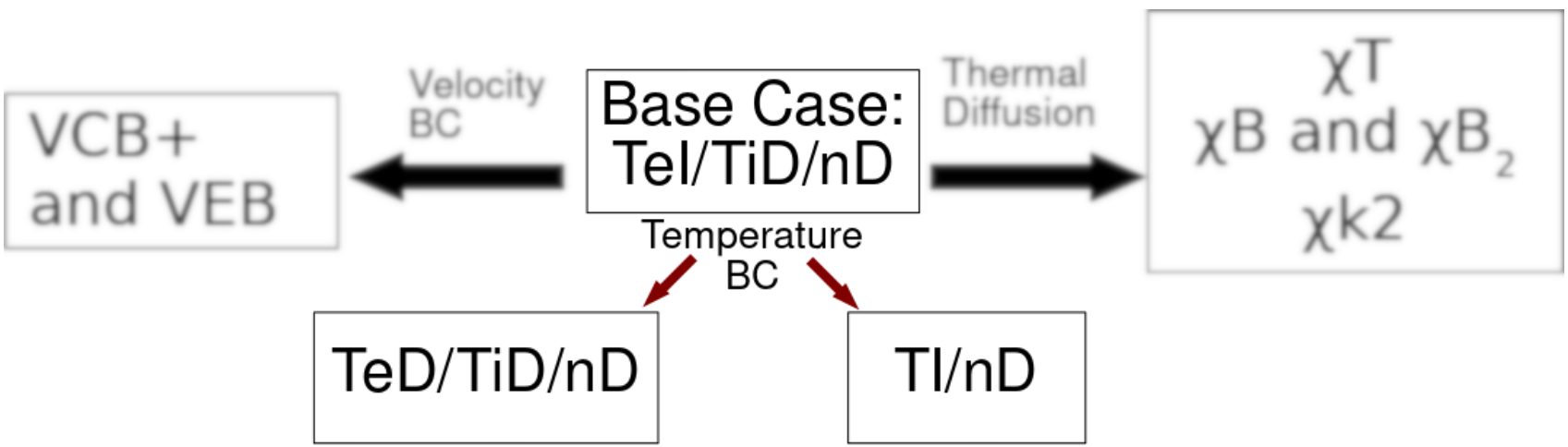

Applying insulating conditions lengthens the plasma termination time.

- The single-T insulating case lasts the longest and the Dirichlet conditions with cold walls decay fastest.

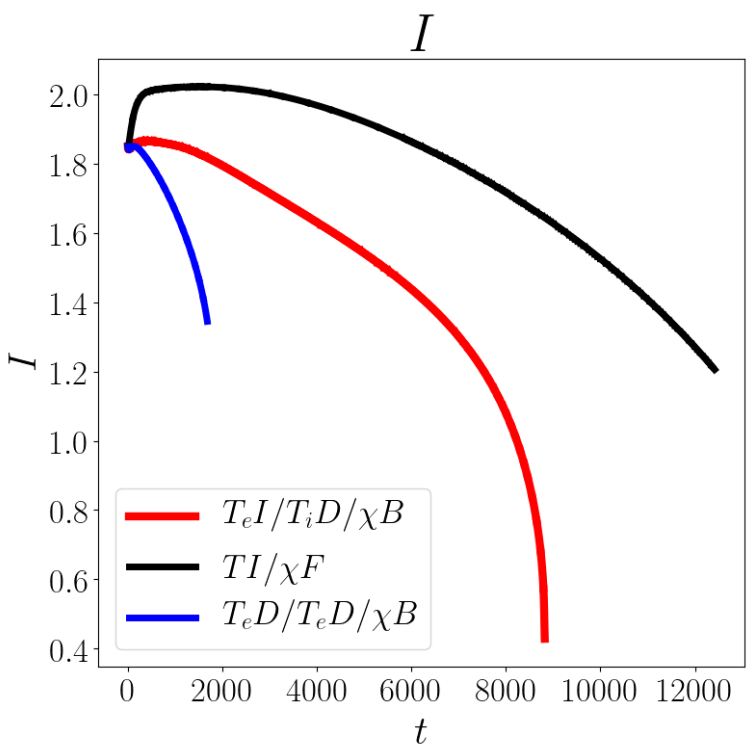

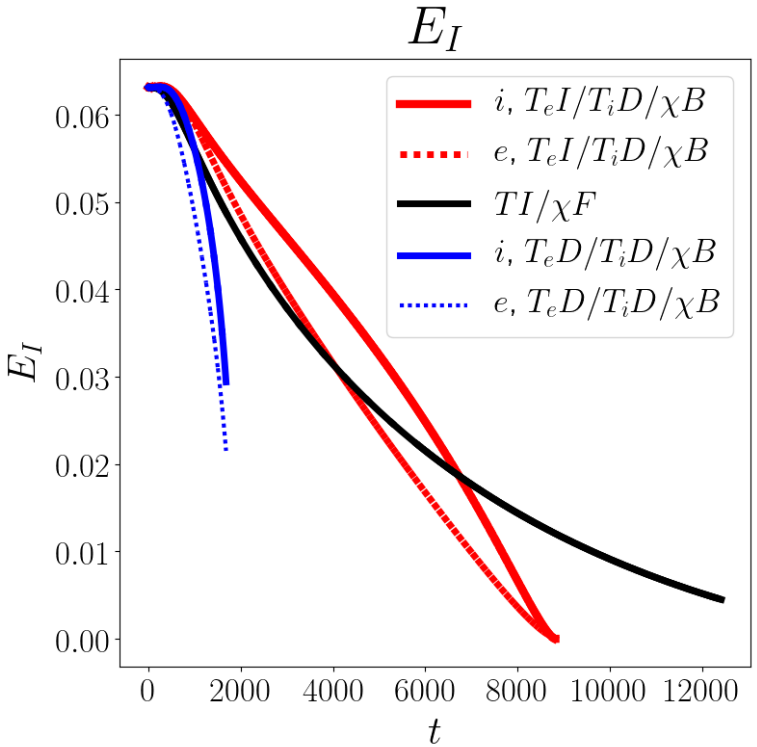

Vertical forces are also affected by these boundary conditions.

- The two Chodura-Bohm cases have clear termination times where the force peaks.
- When extrapolated to ITER, the equivalent vertical force would be on the order of 10 MN

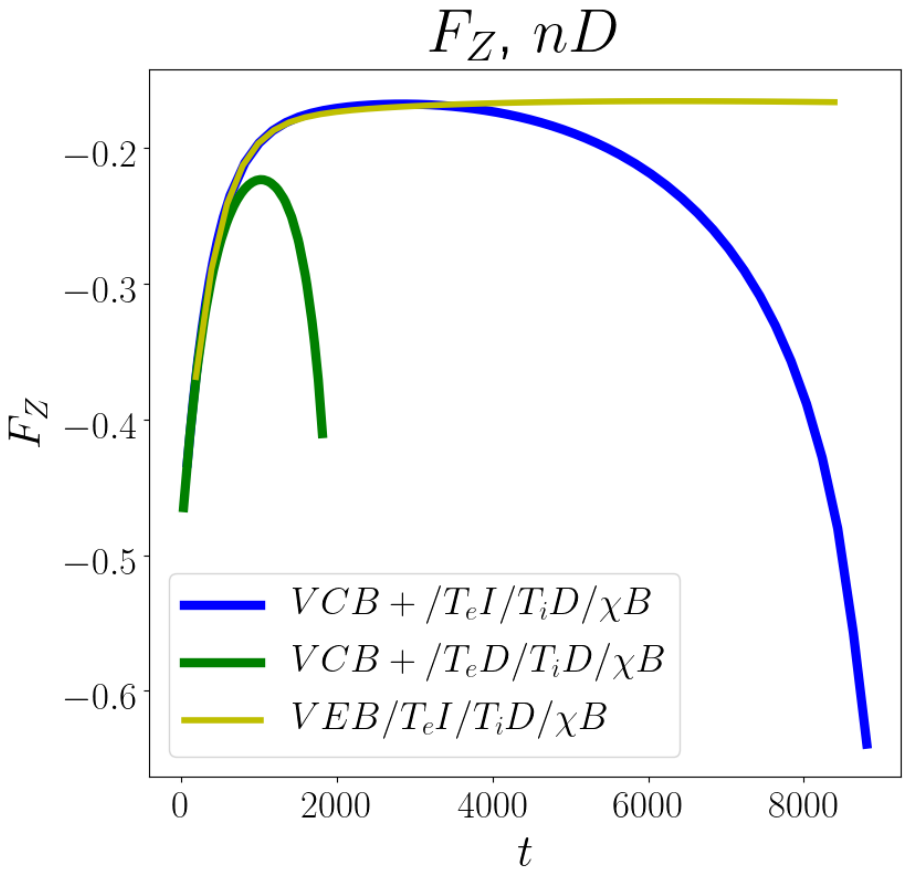

The distribution of the force over the wall is highly concentrated at the plasma contact point.

- The distribution of the force along the wall shows a large concentration near the plasma-wall contact point.

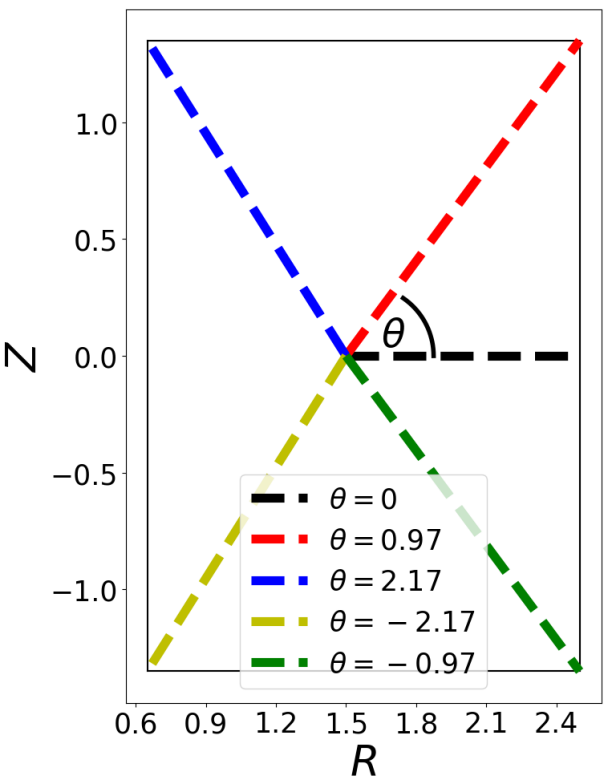

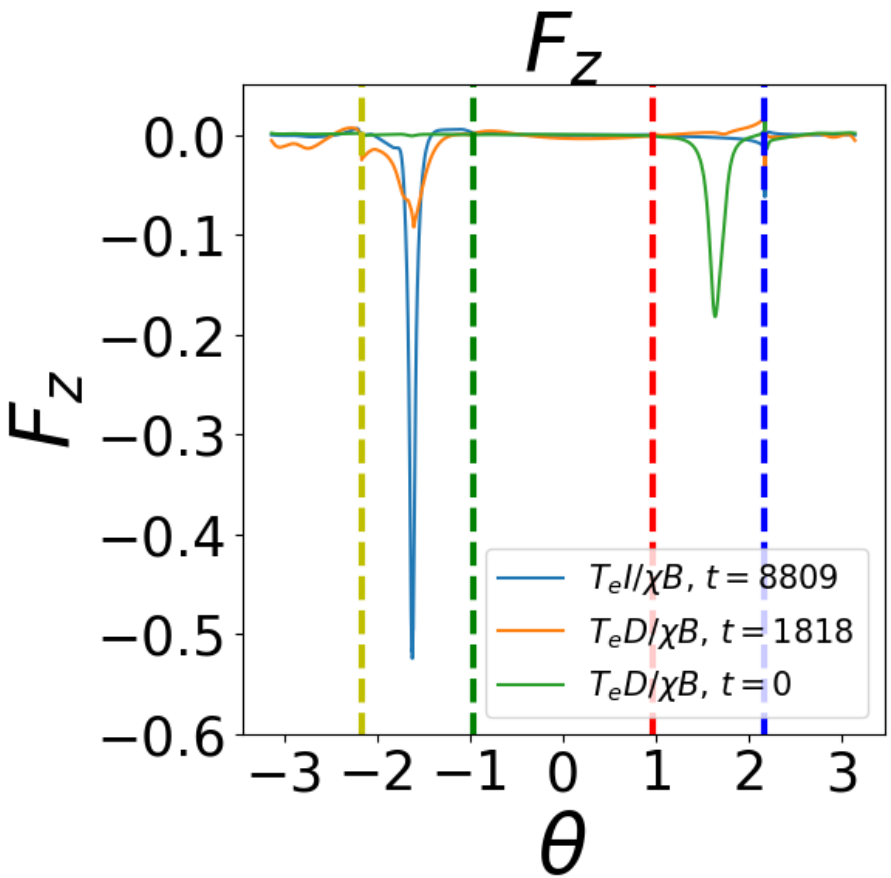

Table of Contents

Conclusions

- The edge boundary conditions and thermal conduction models affect the halo region's temperature and resistivity which affects the VDE motion.
- VDE sensitivity to boundary conditions and thermal conduction models prompts us to apply more detailed modeling.
- The most comprehensive model using Braginskii thermal conduction is more robust numerically, and does not require tuning.

Future Work

- An ion saturation current condition is needed to complete the MPS boundary conditions.
- Radiation from impurities and the effects of neutrals will affect edge conditions.
- Non-axisymmetric cases should be run and the associated horizontal and vertical forces calculated.

The k2 model functions.

$$\chi_{\parallel,e} = \frac{T_e \tau_e}{m_e} \hat{k}_{\parallel,e}$$

$$\chi_{\perp,e} = \frac{T_e \tau_e}{m_e} \frac{(\frac{13}{4}\zeta + \sqrt{2}) x_e + \hat{k}^{(1)}_{\perp,e} \hat{k}_{\parallel,e}}{x_e^3 + \hat{k}^{(5)}_{\perp,e} x_e^{7/3} + \hat{k}^{(4)}_{\perp,e} x_e^2 + \hat{k}^{(3)}_{\perp,e} x_e^{5/3} + \hat{k}^{(2)}_{\perp,e} x_s + \hat{k}^{(1)}_{\perp,e}}$$

$$\tau_e = \tau_{ei}$$

$$\hat{k}_{\parallel,e} = \frac{13.5 Z_{\text{eff}}^2 + 54.4 Z_{\text{eff}} + 25.2}{Z_{\text{eff}}^3 + 8.35 Z_{\text{eff}}^2 + 15.22 Z_{\text{eff}} + 4.5} \overset{Z_{\text{eff}}=1}{=} 3.204$$

$$\hat{k}^{(1)}_{\perp,e} = \frac{9.91 Z_{\text{eff}}^3 + 75.32 Z_{\text{eff}}^2 + 518 Z_{\text{eff}} + 333}{1000} \overset{Z_{\text{eff}}=1}{=} 0.936$$

$$\hat{k}^{(2)}_{\perp,e} = \frac{0.211 Z_{\text{eff}}^3 + 12.7 Z_{\text{eff}}^2 + 48.4 Z_{\text{eff}} + 6.45}{Z_{\text{eff}} + 57.1} \overset{Z_{\text{eff}}=1}{=} 1.166$$

$$\hat{k}^{(3)}_{\perp,e} = \frac{0.932 Z_{\text{eff}}^{7/3} + 0.135 Z_{\text{eff}}^2 + 12.3 Z_{\text{eff}} + 8.77}{Z_{\text{eff}} + 4.84} \overset{Z_{\text{eff}}=1}{=} 3.791$$

$$\hat{k}^{(4)}_{\perp,e} = \frac{0.246 Z_{\text{eff}}^3 + 2.65 Z_{\text{eff}}^2 - 92.8 Z_{\text{eff}} - 1.96}{Z_{\text{eff}}^2 + 19.9 Z_{\text{eff}} + 35.3} \overset{Z_{\text{eff}}=1}{=} -1.635$$

$$\hat{k}^{(5)}_{\perp,e} = \frac{2.76 Z_{\text{eff}}^{5/3} - 0.836 Z_{\text{eff}}^{2/3} - 0.611}{Z_{\text{eff}} - .214} \overset{Z_{\text{eff}}=1}{=} 2.370$$

$$\chi_{\parallel,i} = \frac{T_i \tau_i}{m_i} \hat{k}_{\parallel,i}$$

$$\chi_{\perp,i} = \frac{T_i \tau_i}{m_i} \frac{(\frac{15}{2}\zeta + \sqrt{2}) x_i^2 + 0.1693 \hat{k}_{\parallel,i} (\Delta_{\parallel,i})^2}{\Delta_{\perp,i}}$$

$$\tau_i = \tau_{ii}$$

$$\hat{k}_{\parallel,i} = \frac{5.524 + 30.38\zeta}{\Delta_{\parallel,i}}$$

$$\Delta_{\parallel,i} = 1 + 13.50\zeta + 36.46\zeta^2$$

$$\Delta_{\perp,i} = x_i^4 + (1.352 + 12.49\zeta + 34\zeta^2) x_i^2 + 0.1693 (\Delta_{\parallel,i})^2$$

$$\zeta = \frac{1}{Z_{\text{eff}}} \sqrt{\frac{m_e}{m_i} \frac{T_i}{T_e}}$$